ARTICLE

Resonance Raman Spectroscopic and Theoretical Study of Geometry Distortion of Thiourea in 2^1A State

Hai-bo Zhang, Yan-ying Zhao, Xu-ming Zheng*

Department of Chemistry, State Key Laboratory of advanced Textiles Materials and Manufacture Technology, MOE, Zhejiang Sci-Tech University, Hangzhou 310018, China

(Dated: Received October 2, 2011; Accepted on November 22, 2011)

The A-band resonance Raman spectra of thiourea were obtained in water and acetonitrile solution. B3LYP/6-311++G(3df,3pd) and RCIS/6-311++G(3df,3pd) calculations were done to elucidate the ultraviolet electronic transitions, the distorted geometry structure and the saddle point of thiourea in 2^1A excited state, respectively. The resonance Raman spectra were assigned. The absorption spectrum and resonance Raman intensities were modeled using Heller's time-dependent wavepacket approach to resonance Raman scattering. The results indicate that largest change in the displacement takes place with the C=S stretch mode ν_6 ($|\Delta|$=0.95) and noticeable changes appear in the $H_5N_3H_6$+$H_8N_4H_7$ wag ν_5 ($|\Delta|$=0.19), NCN symmetric stretch+C=S stretch+N_3H_6+H_8N_4 wag ν_4 ($|\Delta|$=0.18), while the moderate intensities of $2\nu_{15}$ and $4\nu_{15}$ are mostly due to the large excited state frequency changes of ν_{15}, but not due to its significant change in the normal mode displacement. The mechanism of the appearance of even overtones of the $S{=}CN_2$ out of plane deformation is explored. The results indicate that a Franck-Condon region saddle point is the driving force for the quadric phonon mechanism within the standard A-term of resonance Raman scattering, which leads to the pyramidalization of the carbon center and the geometry distortion of thiourea molecule in 2^1A excited state.

Key words: Thiourea, Excited state structural dynamics, Resonance Raman, Time-dependent wavepacket approach, Density functional theory

I. INTRODUCTION

The N-V band system in the 6.0−8.5 eV region of the UV spectrum of alkenes was first characterized by Mulliken as resulting from a $\pi_{C=C}\rightarrow\pi^*_{C=C}$ transition of the C=C double bond, where N and V were defined as $^1\pi^2$ and $^1\pi\pi^*$ states respectively [1]. Alkenes in the $^1\pi\pi^*$ state usually quickly depart their planar geometries and leads to a perpendicular orientation of the vicinal groups with respect to each other that shows two near-degenerate excited state potential energy surfaces in the vicinity of the perpendicular geometry of alkenes [1]. The excited state conformational rotation around C=C double bond of alkenes induces a "sudden polarization" effect for alkenes [2, 3]. A large number of studies have been carried out to explore the generality of "sudden polarization" effect existed in a wide variety of olefins in the vicinity of their perpendicular geometry [4−12]. According to theoretical studies, the occurrence of the sudden polarization phenomenon in symmetrical alkenes is generally assumed to be driven by an exothermic intramolecular symmetry-lowering perturbation (*e.g.* a selective pyramidalization of one of the olefinic carbon centers) [3, 6, 7], and the avoided crossing between the two potential energy surfaces [13−16]. Resonance Raman studies on ethylene has been demonstrated that strong vibronic coupling exists in the $^1\pi\pi^*$ state with the torsional vibration being the primary active mode [17−19]. These studies reveal that the $^1\pi\pi^*$ state is not only twisted, but also pyramidalized about the carbon atoms and the torsional vibrational mode is a Raman indicator for the excited state torsional motion that leads to a perpendicular orientation of the vicinal groups.

Recently resonance Raman spectroscopy was used to explore the excited state structural dynamics of methyl xanthate anion $CH_3OCS_2^-$ that displays a conformational deformation and a pyramidalization of the carbon center upon photoexcitation [20]. Methyl xanthate anion has its own functional group $-CS_2^-$ in which two C=S double bonds conjugate together to form a conjugated π system which is in nature different from the single C=C double bond of alkenes. Our resonance Raman spectroscopic and random chip-interleaving system (RCIS) computational results indicate that the Franck-Condon region saddle point is the driving force for the appearance of the even overtone of the OCS_2 out-of-

*Author to whom correspondence should be addressed. E-mail: zxm@zstu.edu.cn

plane deformation.

In this work, we study the further resonance Raman and quantum mechanical computational studies of the excited state structural dynamics of thiourea ($S{=}C(NH_2)_2$). Thiourea is an interesting molecule where the non-bonding electrons in two NH_2 groups involve significantly in the conjugations with the $\pi_{C=S}$ and $\pi^*_{C=S}$ orbitals. The similar pyramidalization of the carbon center in thiourea upon photoexcitation is examined. The absorption spectrum and resonance Raman intensities were modeled using Heller's time-dependent wavepacket approach. It is further proved that the excited state conformational out-of-plane deformation motion of the molecule is driven by a saddle point in Franck-Condon region.

II. EXPERIMENTAL AND COMPUTATIONAL METHODS

A. Experiments

Solid-state FT-Raman and FT-IR spectra of thiourea were obtained using Thermo Nicolet FT-Raman 960 spectrometer and Perkin-Elmer 1 FT-IR spectrometer. The UV absorption spectrum of thiourea in water was measured using ultraviolet/visible spectrometer. The resonance Raman experimental methods and apparatus have been described previously [21−23] so only a short description will be provided here. The harmonics of a nanosecond Nd:YAG laser and their hydrogen Raman shifted laser lines were employed to generate the 245.9 and 252.7 nm excitation wavelengths utilized in the resonance Raman experiments. Concentrations of approximately 3.2 mL/(mol cm) thiourea (99% purity) in redistilled water solvent were used to prepare sample solutions. The excitation laser beam used a ∼100 μJ pulse energy loosely focused to a 0.5−1.0 mm diameter spot size onto a flowing liquid stream of sample to excite the sample. Power-dependent experiments were done using ∼100 μJ pulse energy focused on a beam diameter of ∼1.0 mm and ∼260 μJ pulse energy focused on a beam diameter of ∼0.5 mm respectively. No power-dependent Raman peaks were found within the test conditions and this indicated that there were no noticeable transients or photoproducts contributed to the resonance Raman spectra.

A backscattering geometry was employed for collection of the Raman scattered light by reflective optics that imaged the light through a polarizer and entrance slit of a 0.5 m spectrograph and the grating of the spectrograph dispersed the light onto a liquid nitrogen cooled charge coupled decice (CCD) mounted on the exit of the spectrograph. The CCD accumulated the Raman signal for about 120 s before being read out to an interfaced PC computer with 30 of these scans added together to get the resonance Raman spectrum. The Raman shifts of the resonance Raman spectra were calibrated with the known vibrational frequencies of the acetonitrile solvent Raman bands and the solvent Raman bands were then subtracted from the resonance Raman spectra by utilizing an appropriately scaled solvent spectrum. Sections of the resonance Raman spectra were fit to a baseline plus a sum of Lorentzian bands to determine the integrated areas of the Raman bands of interest. The FT-IR and FT-Raman spectra of thiourea in the neat solid were acquired so as to do a vibrational analysis that could be used to help make vibrational assignments for the resonance Raman spectra.

Depolarization ratio measurements were done with a Glan Prism polarizer that was placed in the scattered beam just before the entrance slit of the spectrograph [24] and the polarization response of the spectrometer was referenced to measurements of the cyclohexane bands that were employed as a standard. The three depolarized bands at 1347, 1226, and 1027 cm^{-1} gave the depolarization ratio ρ values of 0.75±0.05, while that for the 802 cm^{-1} band was 0.13±0.01. These values suggest that the measured values for thiourea are not affected by the polarization dependence of the grating efficiency nor by any appreciable leak of the polarization analyzer. ρ of the Raman fundamentals and overtones and combination bands for thiourea in acetonitrile were measured to be close to $\rho{\approx}0.33$ and the results were listed in Table S1 in supplementary materials. The absolute Raman cross sections of the resonance Raman spectra of thiourea were determined relative to the 2249 cm^{-1} Raman band of the CH_3CN solvent.

B. Calculation

The absorption spectrum and resonance Raman intensities were modeled using Heller's time-dependent wavepacket approach [24−27] with the absorption spectrum computed using the following expression:

$$\sigma_A(E_L) = \frac{4\pi e E_L M_0^2}{3n\hbar c}\int_{-\infty}^{\infty} G(\delta)\mathrm{d}\delta \mathrm{Re}\int_0^{\infty}\mathrm{d}t\langle 0|0(t)\rangle\cdot \exp\left[\frac{i(E_L+\varepsilon_0)t}{\hbar}\right]\exp\left(\frac{-\Gamma t}{\hbar}\right) \quad (1)$$

and the resonance Raman intensities computed with the following formula:

$$\sigma_R(E_L) = \frac{8\pi e^4 E_S^3 E_L M_0^4}{9\hbar^6 c^4}\int_{-\infty}^{\infty} G(\delta)\mathrm{d}\delta\left|\int_0^{\infty}\mathrm{d}t\langle f|0(t)\rangle\cdot \exp\left[\frac{i(E_L+\varepsilon_0)t}{\hbar}\right]\exp\left(\frac{-\Gamma t}{\hbar}\right)\right|^2 \quad (2)$$

where E_L is the incident photon energy, M_0 is the transition dipole moment evaluated at the equilibrium geometry, f is the final state for the Raman scattering, and n is the solvent index of refraction. The term $\exp(-t\Gamma/\hbar)$ is a homogeneous damping function that has contributions from the excited state population decay and pure dephasing. $\delta{=}\hbar(\varpi_0{-}\omega_0)$ is the shift from

DOI:10.1088/1674-0068/25/01/1-10

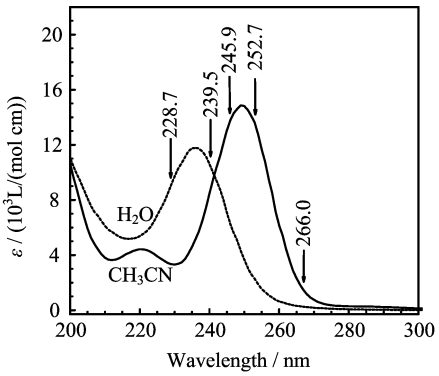

FIG. 1 UV absorption spectra of thiourea in water and acetonitrile solvents with the excitation wavelengths for the resonance Raman experiments indicated above the spectra.

the central zero-zero frequency ϖ_0 due to inhomogeneous broadening, and

$$G(\delta)=\frac{1}{\theta}\sqrt{2\pi}\exp\left(\frac{-\delta^2}{2\theta^2}\right) \quad (3)$$

which is a normalized Gaussian distribution of site electronic energies. $|0(t)\rangle=e^{-iHt/\hbar}|0\rangle$ which is $|0\rangle$ propagated on the excited state surface for a time t and H is the excited state vibrational Hamiltonian.

Geometry optimization and vibrational frequency computations were done using the B3LYP/6-311++G(3df,3pd) level of theory with C_s symmetry for ground state thiourea and RCIS/6-311++G(3df,3pd) level of theory without the C_s symmetry for $S_2(^1\pi\pi^*)$ excited state thiourea, while the electronic transition energies were calculated using B3LYP-TD/6-311++G(3df,3pd) method. All the calculations were carried out in Gaussian 03 program [28].

III. RESULTS AND DISCUSSION

A. UV spectra

Figure 1 shows the UV absorption spectra of thiourea in water and acetonitrile solvents with the excitation wavelengths for the resonance Raman experiments indicated above the spectra. The spectra in water and acetonitrile solvent display respectively an intense A-band absorption at ∼236 nm (molar extinction coefficient ε=14858 L/(mol cm), f=0.25) and ∼249 nm (ε=117802 L/(mol cm), f=0.31). To simulate the solvent effects on the UV spectra of thiourea in solvents, the B3LYP-TD/6-311++G(3df,3pd) level of theory calculations employing PCM solvent model were carried out. Table I lists the computed electronic transition energies and the oscillator strengths of thiourea, while Fig.2 depicts the molecular orbitals associated with the calculated electronic transitions.

To ease the understanding of the electronic structures of the excited states in gas phase, six frontier molecular

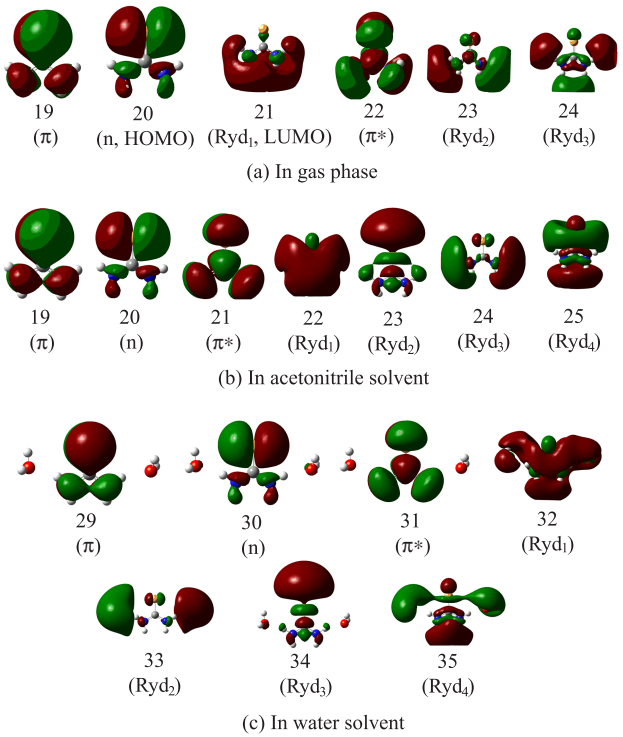

FIG. 2 Molecular orbitals associated with the electronic transitions of thiourea as listed in Table I.

orbitals are briefly characterized in Fig.2(a). The highest occupied molecular orbital 20 (HOMO) is a nonbonding orbital of C=S group with large amplitudes localized on the S atom. The second highest occupied MO 19 is a π orbital delocalized into whole molecule. The lowest-lying unoccupied MO 21 (LUMO) is a diffuse orbital (designated by Ryd_1). The second lowest-lying unoccupied MO 22 is a π^* orbital. The remaining two lowest-lying unoccupied MOs are respectively the Ryd_2 and the Ryd_3. Similarly, seven frontier molecular orbitals associated with the electronic transitions of thiourea in solvents of acetonictrile and water are also characterized in Fig.2 (b) and (c).

Table I show that the transition energies of n→Ryd_n and π→Ryd_n transitions are very sensitive to the solvations. For example, the transition energy of n→Ryd_3 for $S_5(3^1B)$ state in gas phase is located at 226 nm, and it disappears in water and acetonitrile solvents. Similarly, the transition energy of π→Ryd_1 for $S_3(2^1B)$ state in gas phase is located at 265 nm, which blue-shifts to 229 nm in acetonitrile and 233 nm in water. Most of the calculated n→Ryd_n and π→Ryd_n transitions that have relative larger oscillator strengths in gas phase blue-shift significantly. This simplifies the comparison between the experimental UV spectra and the calculated ones in solution phases. Therefore the experimental bands at 249 nm (most intense band) and 220 nm (moderate intense) in acetonitrile are tentatively assigned as the π→π^* transition ($S_2(2^1A)$) and n→Ryd_1 transition

DOI:10.1088/1674-0068/25/01/1-10

TABLE I B3LYP-TD/6-311++G(3df,3pd) computed electronically singlet transition energy of thiourea in gas phase, in acetonitrile, and water solvents.

	States	Transition energy/nm		Transition	$\langle f \rangle$		Orbitals(coefficient)
		Calc.	Expt.		Calc.	Expt.	
A[a]	$S_1(2^1A)$	316		$n\rightarrow\pi^*$	0.0001		20→22 (0.688)
	$S_2(1^1B)$	283		$n\rightarrow Ryd_1$	0.0320		20→21 (0.702)
	$S_3(2^1B)$	265		$\pi\rightarrow Ryd_1$	0.0037		19→21 (0.702)
	$S_4(3^1A)$	247		$\pi\rightarrow\pi^*$	0.0874		19→22 (0.536)
				$n\rightarrow Ryd_2$	0.0874		20→23 (−0.396)
	$S_5(3^1B)$	226		$n\rightarrow Ryd_3$	0.0465		20→24 (0.697)
				$\pi\rightarrow\pi^*$	0.0465		19→22 (0.322)
	$S_6(4^1A)$	226		$\pi\rightarrow Ryd_2$	0.1141		19→23 (0.246)
				$n\rightarrow Ryd_2$	0.1141		20→23 (0.536)
	$S_7(5^1A)$	221		$\pi\rightarrow Ryd_2$	0.0409		19→23 (0.652)
	$S_8(4^1B)$	214		$\pi\rightarrow Ryd_3$	0.0155		19→24 (0.698)
B[b]	$S_1(1^1A)$	273		$n\rightarrow\pi^*$	0.000		20→21 (0.701)
	$S_2(2^1A)$	237	249	$\pi\rightarrow\pi^*$	0.22	0.31	19→21 (0.658)
	$S_3(1^1B)$	233	220	$n\rightarrow Ryd_1$	0.0876		20→22 (0.698)
	$S_4(2^1B)$	229		$\pi\rightarrow Ryd_1$	0.02		19→22 (0.702)
	$S_5(3^1B)$	207		$n\rightarrow Ryd_3$	0.0005		20→23 (0.683)
				$n\rightarrow Ryd_4$	0.0005		20→25 (0.120)
	$S_6(4^1B)$	202		$\pi\rightarrow Ryd_2$	0.005		19→23 (0.678)
				$\pi\rightarrow Ryd_4$	0.005		19→25 (0.151)
	$S_7(4^1A)$	190		$\pi\rightarrow Ryd_3$	0.000		19→24 (0.661)
C[c]	S_1	271		$n\rightarrow\pi^*$	0.000		30→31 (0.701)
	S_2	240	236	$n\rightarrow Ryd_1$	0.100	0.25	30→32 (0.698)
	S_3	235	236	$\pi\rightarrow\pi^*$	0.203	0.25	29→31 (0.659)
	S_4	233		$\pi\rightarrow Ryd_1$	0.02		29→32 (0.702)
	S_5	209		$n\rightarrow Ryd_2$	0.0014		30→33 (0.605)
				$n\rightarrow Ryd_3$	0.0014		30→34 (−0.322)
	S_6	208		$n\rightarrow Ryd_2$	0.0004		30→33 (0.659)
				$n\rightarrow Ryd_3$	0.0004		30→34 (0.659)
	S_7	206		$\pi\rightarrow Ryd_2$	0.000		29→33 (0.700)
	S_8	202		$\pi\rightarrow Ryd_3$	0.005		29→34 (0.669)

[a] At B3LYP-TD/6-311++G(3df,3pd) level of theory for thiourea in gas phase (for molecular orbitals associated the electronic transitions listed below see Fig.2(a)).
[b] At B3LYP-TD/6-311++G(3df,3pd) level of theory for thiourea in acetonitrile solvent employing PCM solvent model (for molecular orbitals associated the electronic transitions listed below see Fig.2(b)).
[c] At B3LYP-TD/6-311++G(3df,3pd) level of theory for thiourea-water cluster in water solvent employing PCM solvent model (for molecular orbitals associated the electronic transitions listed below see Fig.2(c)).

($S_3(1^1B)$), while the experimental 236 nm band in water is tentatively assigned as a mixed $\pi\rightarrow\pi^*$ and $n\rightarrow Ryd_1$ transitions.

The three excited electronic states A, B, and C, which correspond respectively to the 250, 220, and 197 nm bands of thiourea in acetonitrile, were previously investigated [29]. Under a C_{2v} symmetry point group, the transition moments of the A- and B-band absorptions are respectively along the z and x directions. The A-band at 250 nm, B-band at 220 nm, and C-band at 197 nm were respectively assigned to $\pi_{CS}\pm(\pi_N+\pi_N)\rightarrow\pi^*_{CS}$ (a_1 symmetry), $(\pi_N-\pi_N)\rightarrow\pi^*_{CS}$ (b_1 symmetry), and $\pi_{CS}\rightarrow\pi^*_{CS}$ (a_1 symmetry). The assignment of the A-band absorption in acetonitrile to $\pi_{CS}\pm(\pi_N+\pi_N)\rightarrow\pi^*_{CS}$ (a_1 symmetry) is supported by our assignment, as listed in Table I, while the assignment of the B-band absorption to $(\pi_N-\pi_N)\rightarrow\pi^*_{CS}$ (b_1 symmetry) seems not consistent with the $n\rightarrow Ryd_1$ assignment, as predicted by our B3LYP-TD/6-311++G(3df,3pd) level of theory calculations employing polarizable continuum model (PCM) solvent model.

DOI:10.1088/1674-0068/25/01/1-10

TABLE II B3LYP/6-311++G(3df,3pd) calculated and experimentally (FT-Raman and FT-IR) observed vibrational frequencies of thiourea, units in cm^{-1}.

Mode	Calculated		FT-Raman		FT-IR			Description
	a*	b*	This work	Ref.[33]	This work	Ref.[36]	Ref.[35]	
ν_1	3697	3657				3682		$H_5N_3H_6$ stretch+$H_8N_4H_7$ stretch
ν_2	3571	3532				3539		$H_5N_3H_6$ stretch+$H_8N_4H_7$ stretch
ν_3	1651	1633	1636			1613	1610	$H_5N_3H_6$ scissor+$H_8N_4H_7$ scissor
ν_4	1405	1390	1384	1378		1391	1401	NCN symmetric stretch+C=S stretch+ N_3H_6+H_8N_4 wag
ν_5	1063	1051	1094	1105	1085	1053	1078	$H_5N_3H_6$ wag+$H_8N_4H_7$ wag
ν_6	770	760	735	744	730	758	760	C=S stretch
ν_7	477	470	480			476		N_3H_5 and N_4H_7 rock
ν_8	459	454					459	NCN scissor
ν_9	307	303				307		N_3H_6 and N_4H_8 rock
ν_{10}	3696	3656						$H_5N_3H_6$ stretch+$H_8N_4H_7$ stretch
ν_{11}	3563	3524						$H_5N_3H_6$ stretch+$H_8N_4H_7$ stretch
ν_{12}	1625	1607	1612	1627	1616	1592	1583	$H_5N_3H_6$ scissor+$H_8N_4H_7$ scissor
ν_{13}	1422	1405		1391	1416	1412		NCN anti-symmetric stretch
ν_{14}	1063	1051			1086			$H_5N_3H_6$ wag+$H_8N_4H_7$ wag
ν_{15}	641	633			633		645	S=CN_2 out of plane rock
ν_{16}	581	574	573	562				N_3H_5 and N_4H_7 rock
ν_{17}	400	395	385					C=S wag
ν_{18}	362	358	355					N_3H_6+N_4H_8 rock

* a: B3LYP/6-311++G(3df,3pd) calculated; b: Scaled=0.989 calculated.

B. Resonance Raman spectra and vibrational assignments

Several investigations on the vibrational band assignments of the thiourea have been reported previously [29−36]. A detailed vibrational analysis on the structure of pure thiourea were carried out recently on the basis of the assumption that the molecule has C_{2v} point group symmetry [34]. However, the searching of the potential energy surface (PES) of thiourea for stable conformers under C_1, C_s, C_2, and C_{2v} symmetry constraints by using the theories of second-order Moeller-Plesset perturbation (MP2) and quadratic configuration interaction with single and double excitations (QCISD) revealed that thiourea conformers of C_2 and C_s symmetry were the stationary points on the PES with no imaginary frequencies at MP2/6-311G(d,p) level, whereas only the C_2 conformer seems as true minimum when basis sets containing more polarization and/or diffuse functions were used [36]. Therefore to ambiguously assign the resonance Raman spectra of thiourea, a revised vibrational assignments have been done in present work on the basis of C_2 point group symmetry and the density functional theory computations. Table II lists the comparison of the B3LYP/6-311++G(3df,3pd) calculated vibrational frequencies to the experimental FT-Raman and FT-IR values. The vibrational assignments have made use of the previous notations and the data, as indicated in Table II. The overall agreement between the linear regression scaled DFT calculated vibrational frequencies and the experimental values is good for thiourea.

The resonance Raman spectra of thiourea in H_2O and D_2O solutions were previously reported using 514.5, 488.0, 457.9, 363.8, 325.0, and 257.3 nm laser beam excitations [29]. The A-band ($\pi_{C=S}\rightarrow\pi^*_{C=S}$) resonance Raman excitation profile of the 729 cm^{-1} line has been examined. The depolarization ratio value of this line was measured to be ρ=0.33. It was concluded that the C=S stretching vibration at 729 cm^{-1} derives its intensity solely from the A-band absorption, while the higher-frequency Raman bands like the NCN antisymmetric stretching vibration at 1520 cm^{-1}, which dominates the 363.8−514.5 nm Raman spectra, are not contributed from the A-band absorption. We have obtained the resonance Raman spectra of thiourea in water and acetonitrile solvents at five laser excitations that cover mostly the experimental absorption bands (∼236 nm in water and ∼250 nm in acetonitrile) of thiourea. Figure 3 displays the overall views of the 228.7, 239.5, 245.9, 252.7, and 266.0 nm resonance Raman spectra in solvents of acetonitrile and water. The comparison of the 239.5 nm resonance Raman spectrum in acetonitrile solution with the FT-Raman spectrum is also displayed in Fig.4. The dashed line in Fig.4 shows the correlation of the Raman peaks in the FT-Raman spectrum to those in 239.5 nm resonance Raman spectrum.

DOI:10.1088/1674-0068/25/01/1-10

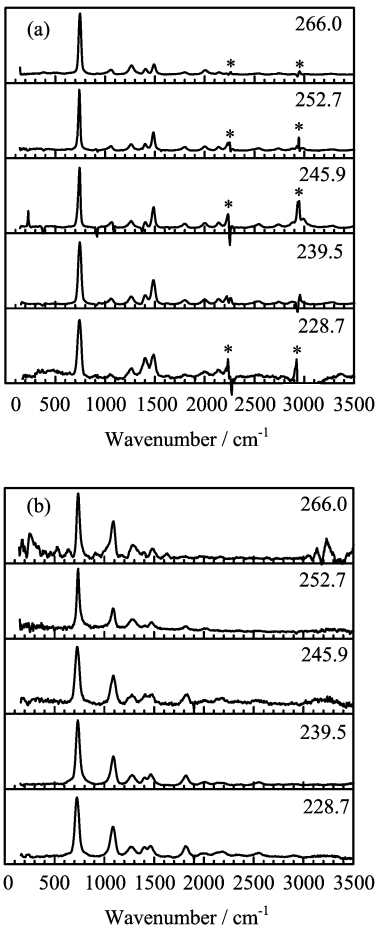

FIG. 3 Comparison of the 228.7, 239.5, 245.9, 252.7, and 266.0 nm resonance Raman spectrum of thiourea in acetonitrile (a) and water solution (b). The resonance Raman spectrum has been intensity-corrected and solvent-subtracted. The asterisks (*) label the regions where solvent subtraction are made.

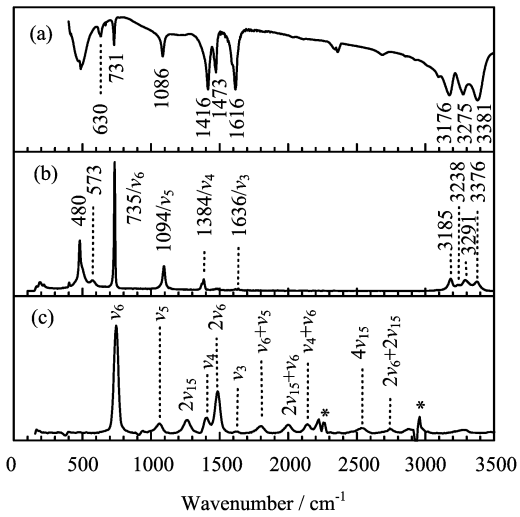

FIG. 4 Comparison of the 239.5 nm resonance Raman spectrum of thiourea in acetonitrile solution with the FT-Raman and FT-IR spectra of thiourea in solid state. The resonance Raman spectrum has been intensity-corrected and solvent-subtracted. (a) FT-IR, (b) FT-Raman, and (c) resonance Raman in CH_3CN. The asterisks (*) mark solvent subtraction artifacts.

Figure 4 indicates that the intensity patterns are very different between FT-Raman spectrum and 239.5 nm resonance Raman spectrum. The most important difference is the appearance of the new band at $\sim$1260 cm^{-1} for 239.5 nm resonance Raman spectrum. This band is not observed in the FT-Raman spectrum, and is assigned to the first overtone $2\nu_{15}$ of the calculated out-of-plane mode ν_{15} at $\sim$633 cm^{-1} (B irreducible representative). The Raman transitions of $4\nu_{15}$ and $2\nu_{15}+\nu_6$ are also obvious in the 239.5 nm resonance Raman spectra. $3\nu_{15}$ is not observed near 1900 cm^{-1}. Most of the resonance Raman intensity of the 239.5 nm resonance Raman spectrum in acetonitrile solvent can be assigned to the fundamentals, overtones and combination bands of five Franck-Condon active vibrational modes. They are the C=S stretch (ν_6, 735 cm^{-1}), the $H_5N_3H_6$+$H_8N_4H_7$ wag (ν_5, 1061 cm^{-1}), NCN symmetric stretch+C=S stretch+N_3H_6+H_8N_4 wag (ν_4, 1384 cm^{-1}), the $H_5N_3H_6$+$H_8N_4H_7$ scissor (ν_3, 1636 cm^{-1}), and the overtone of the S=C($-$N)$_2$ out of plane deformation ($2\nu_{15}$, 1260 cm^{-1}). The C=S stretch (ν_6, 744 cm^{-1}) has the largest overtone progressions and forms strong combination bands with other four Franck-Condon active modes (ν_5, ν_4, ν_3, and $2\nu_{15}$). This suggests that the $S_2(^1\pi\pi^*)$ excited state of thiourea in acetonitrile solvent undergoes substantial geometry changes along the reaction coordinators of the C=S stretch, the C$-$N stretch, and the S=C($-$N)$_2$ out of plane deformation. Since the S=C($-$N)$_2$ out of plane deformation vibrational mode belongs to B irreducible representation, it is expected that a significant out-of-plane motion occurs for thiourea in the $S_2(^1\pi\pi^*)$ excited state in Franck-Condon region.

To help understanding the excited state structural dynamics predicted by the 239.5 nm resonance Raman spectrum, the RCIS/6-311++G(3df,3pd) optimized geometry parameters for the $S_2(^1\pi\pi^*)$ excited state are used for comparison. We have noted that RCIS/6-311++G(3df,3pd) optimization may not give the quantitative descriptions of the excited state structure and a quantitative description need more sophisticated quantum mechanical calculations like MRCI and CASSCF method, it still can give us a qualitative information about geometry distortion in excited states. Figure S1 in supplementary material displays the schematic structure diagrams of thiourea in S_0 and $S_2(^1\pi\pi^*)$ excited states. Table III lists the B3LYP/6-311++G(3df,3pd) and RCIS/6-311++G(3df,3pd) calculated bond length and bond angles for S_0, $S_2'(2^1A)$, and $S_{2,min}$ structures. $S_2'(2^1A)$ is an optimized structure under C_2 point group, while $S_{2,min}$ is an optimized structure without symmetry constrain. The computed vibrational spectrum

DOI:10.1088/1674-0068/25/01/1-10

TABLE III B3LYP/6-311++G(3df,3pd) calculated and experimentally observed vibrational frequencies of thiourea.

	S_0	$S_2'(2^1A)$[a]	$S_{2,min}$
R(S=C)	1.66	1.73	1.68
R(C2−N3)	1.36	1.36	1.39
R(C2−N4)	1.36	1.36	1.40
R(N3−H5)	1.00	0.99	0.99
R(N3−H6)	1.01	1.00	0.99
R(N4−H7)	1.00	0.99	0.99
R(N4−H8)	1.01	1.00	1.00
∠S=C−N3	123	120.6	117
∠S=C−N4	123	120.6	117
∠N3−C2−N4	115	118.7	112
∠H5−N3−C2	116	115	114
∠H6−N3−C2	121	117	110
∠H7− N4−C2	116	115	114
∠H8−N4−C2	121	117	114
∠H8−N4−H7	117	113	110
∠H5−N3−H6	117	113	110
D(S1−C2−N3−N4)	180	180	146
D(S1−C2−N3−H5)	−8.6	−14	−41
D(S1−C2−N3−H6)	−159.7	−151	−167
D(S1−C2−N4−H7)	−8.6	−14	−20
D(S1−C2−N4−H8)	−159.7	−151	−77

[a] Saddle point for the S_2 state.

for $S_2'(2^1A)$ structure displays an imaginary frequency that is the S=C−N_2 out-of-plane rock vibrational mode. This indicates that the $S_2'(2^1A)$ structure locates at the saddle point of the potential energy surface for $S_2(^1\pi\pi^*)$ state. Table III shows that while thiourea in ground state has its geometry structure in C_2 symmetry point group, thiourea in S_2 ($^1\pi\pi^*$) excited state has C_1 symmetry point group for minimum structure $S_{2,min}$. This suggests that geometry distortion or symmetry breaking occurs in S_2 ($^1\pi\pi^*$) excited state.

The $^1\pi\pi^*$ state of ethylene is not only strongly twisted, but also pyramidalized about the carbon. This can be explained by an exothermic intramolecular symmetry-lowering perturbation [3, 6, 7] and the avoided crossing between the two potential energy surfaces [13−16]. The resonance Raman study of the $\pi\rightarrow\pi^*$ transition of ethylene further reveals that the pyramidalization is mostly due to the torsional vibration, the C=C stretch vibration, the CH_2 symmetry scissor vibration and their combination with other vibrational modes. Our present study shows that the geometry distortion and the pyramidalization of carbon atom of thiourea in $S_2(2^1A)$ state is mostly due to the $\pi\rightarrow\pi^*$ transition of thiourea, and the motions of the nontotally symmetric S=C($-$N)$_2$ out-of-plane deformation, the totally symmetric C=S stretch and other vibrational modes. The $\pi_{C=S}$ (orbital 19)$\rightarrow\pi^*_{C=S}$ (orbital 21) transition of thiourea in acetonitrile causes respectively the sulfur atom and the carbon atom to decrease and increase its electronic density. The net result is that carbon atom tends to have hybrid sp^3 orbital in S_2 state that leads to the pyramidalization of carbon center in the S=C($-$N)$_2$ group.

To better understand why S=C($-$N)$_2$ out-of-plane deformation motion occurs in Franck-Condon region, the vibrational frequencies at the saddle point and at the minimum of S_2 excited state potential energy surface are examined. Comparison of the structural parameters calculated using B3LYP/6-311++G(3df,3pd) for S_0 state to those calculated by RCIS/6-311++G(3df,3pd) for S_2 state reveals interesting information about the excited state structural changes. The most significant changes in geometry parameters between in S_0 and in saddle point $S_2'(2^1A)$ happens in bond length and bond angle parameters of R(C2=S1), ∠H8−N4−H7/∠H5−N3−H6, ∠H6−N3−C2/∠H8−N4−C2, ∠S1−C2−N3/∠S1−C2−N4, ∠N3−C2−N4. The C=S bond length of thiourea for saddle point S_2' is 1.73 Å, much longer than the corresponding C=S bond length 1.66 Å of thiourea in S_0 state by +0.07 Å. This correlates to the observed intense resonance Raman band for C=S stretch mode ν_6 at 742 cm^{-1} that indicates a large geometry change along the C=S reaction coordinate in Franck-Condon region. The bond angles ∠H8−N4−H7 and ∠H5−N3−H6 for saddle point S_2' is 117°, longer than the corresponding bond angles 113° of the S_0 state by 4°. Similarly, the bond angles changes of ∠H6−N3−C2 and ∠H8−N4−C2 between in S_0 and in saddle point $S_2'(2^1A)$ are 4° (121°−117°). These bond angles changes consists qualitatively with the observed noticeable resonance Raman fundamentals for nominal $H_5N_3H_6$+$H_8N_4H_7$ wag mode ν_5 and its combination band with C=S stretch mode ν_6. The significant dihedral angle changes in D(S1−C2−N3−N4), D(S1−C2−N3−H5), D(S1−C2−N3−H6), D(S1−C2−N4−H7), D(S1−C2−N4−H8) between in S_0 and in $S_{2,min}$ indicate that both the pyramidalization of the carbon center and the geometry distortion of thiourea molecule occurs upon leaving away from the Franck-Condon region. It is interesting to note that the imaginary frequency found for the saddle point has its normal mode description being the nominal S=C($-$N)$_2$ out-of-plane deformation mode. This is in a very good agreement with the resonance Raman observation of the moderate resonance Raman intensities for $2\nu_{15}$ and $4\nu_{15}$. Therefore it appears that a Franck-Condon region saddle point is the driving force for the quadric phonon mechanism within the standard A-term of resonance Raman scattering, which makes the even overtones $2\nu_{15}$ and $4\nu_{15}$ but not the fundamental ν_{15} (B symmetry) become active and gain intensity.

Figure 5 presents the 239.5 nm resonance Raman spectra of thiourea in solvents of water and acetonitrile with vibrational assignments indicated above the spec-

DOI:10.1088/1674-0068/25/01/1-10

TABLE IV Resonance Raman intensity analysis parameters for the time-dependent wave-packet calculations and the resulting vibrational reorganization energies for thiourea. Absolute Raman cross section σ_R ($\times 10^{-8}$ Å^2/molecule).

Mode	Description	Frequency/cm^{-1}		$\|\Delta\|$	λ_v/cm^{-1}
		Ground state	Excited state		
ν_{15}	S=C−N_2 out of plane rock	630	245	0.02	0
ν_6	C=S stretch	742	742	0.95	335
ν_5	$H_5N_3H_6$ wag+$H_8N_4H_7$ wag	1063	1063	0.19	19
ν_4	NCN symmetric stretch+C=S stretch+H_6N_3+H_8N_4 wag	1404	1404	0.18	22

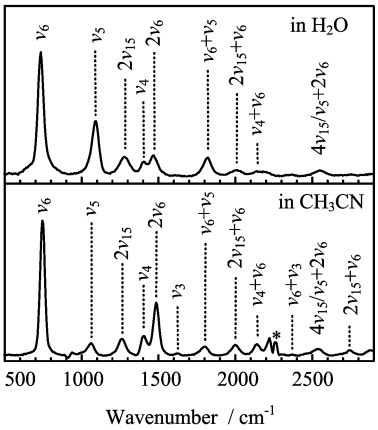

FIG. 5 239.5 nm resonance Raman spectra of thiourea in water and acetonitrile solvents with vibrational assignments indicated above the spectrum. The asterisk (*) marks the solvent subtraction artifact.

tra. Noticeable variations in vibrational frequency of thiourea in two solvents are observed for three Franck-Condon active modes: 735 cm^{-1} in water solvent and 744 cm^{-1} in acetonitrile for the C=S stretch mode ν_6; 1092 cm^{-1} in water and 1061 cm^{-1} in acetonitrile for the $H_5N_3H_6$+$H_8N_4H_7$ wag ν_5; 1277 cm^{-1} in water and 1261 cm^{-1} in acetonitrile for the overtone of the S=C(−N)$_2$ out of plane deformation $2\nu_{15}$. Figure 5 indicates that their intensity patterns are very different. The most important differences lie in the relative intensity $I(\nu_6)/I(2\nu_6)$ and $I(\nu_6)/I(\nu_6+\nu_5)$ in the 239.5 nm resonance Raman spectra of thiourea in water and acetonitrile solvents. It appears that thiourea in acetonitrile solvent undergoes larger geometry change along the C=S bond reaction coordinate relative to in water solvent, while thiourea in water solvent undergoes larger geometry change along the $H_5N_3H_6$+$H_8N_4H_7$ wag ν_5 reaction coordinate relative to in acetonitrile solvent.

C. Simulation of the A-band absorption and resonance Raman spectra

We have chosen to model the relative intensities of the 245.9 and 252.7 nm resonance Raman spectra because they are clearly mostly in resonance with the A-band absorption. The absorption spectrum and absolute resonance Raman cross-section were simulated using the time-dependent wave-packet calculations and a simple model described earlier. Table IV presents the calculated parameters that best fit the absorption spectrum and the intensities of the 245.9 and 252.7 nm resonance Raman spectra for thiourea in acetonitrile solution. To simultaneously fit the absorption bandwidth and the pattern of the resonance Raman intensites, we need to include a large amount of electronic dephasing (the Γ parameter) and a large amount of inhomogeneous broadening (the G parameter) in the calculations. The large Γ parameter indicates that the population decay/electronic dephasing takes place substantially faster than just wavepacket motion away from the Franck-Condon region, while the large G parameter suggests that the broadening of the electronic absorption spectrum is partially because of a number of different salvation structures of thiourea in acetonitrile solution that leads to a distribution of electronic transition energies due to the static interaction between thiourea molecule and acetonitrile solvent.

Figure 6(a) shows a comparison of the computed absorption spectrum with the experimental absorption spectrum, while Fig.6(b) and Table V present comparisons of the computed resonance Raman cross-sections with the experimental Raman cross-sections for the main Raman features of the 245.9 and 252.7 nm resonance Raman spectra. Figure 6 and Table V indicate that the calculated spectrum is consistent with the oscillator strength of the A-band ($\pi_{C=S}\rightarrow\pi^*_{C=S}$) transition while simultaneously providing a good fit to the absolute Raman intensities of the 245.9 and 252.7 nm resonance Raman spectra. The overall best fit to both the absorption spectrum and the absolute resonance Raman intensities appears reasonable enough to extract the major features of the transition and its associated Franck-Condon region structure dynamics on the S_2 excited state potential energy surface. Table IV indicates that largest change in the displacement takes place with the C=S stretch mode ν_6 ($|\Delta|$=0.95) and noticeable changes appear in the $H_5N_3H_6$+$H_8N_4H_7$ wag ν_5 ($|\Delta|$=0.19), NCN symmetric stretch+C=S stretch+N_3H_6+H_8N_4 wag ν_4 ($|\Delta|$=0.18).

DOI:10.1088/1674-0068/25/01/1-10

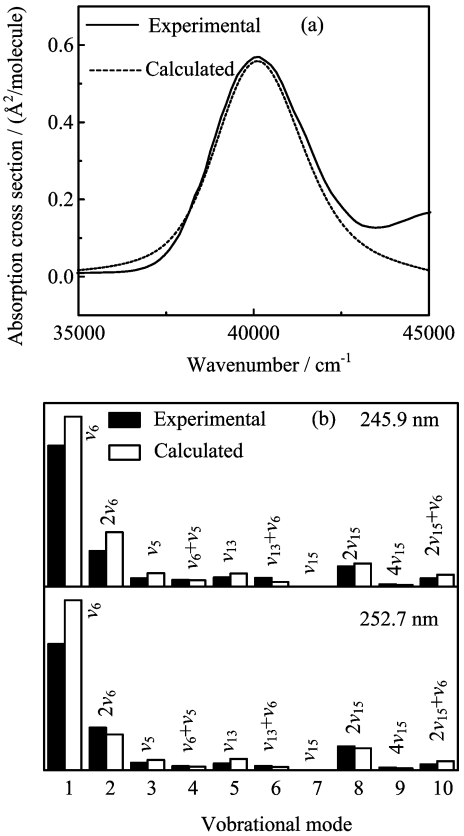

FIG. 6 (a) Comparison of the computed absorption spectrum with the experimental absorption spectrum. (b) Comparison of the computed resonance Raman cross-sections (open bars) with the experimental Raman cross-sections (solid bars) for the main Raman features of the 245.9 and 252.7 nm resonance Raman spectra. The computations made use of the model described in Refs. [24−27] and employed a simple exponential decay dephasing treatment for the solvent.

Since our RCIS calculation indicates that S_2 excited state potential energy surface along the S=C−N_2 out-of-plane rock reaction coordinate (ν_{15}) is a saddle point in the Franck-Condon region, and since our time-dependent wave-packet theory calculations reveals no noticeable normal mode displacement along ν_{15}, the moderate intensities of $2\nu_{15}$ and $4\nu_{15}$ are mostly not due to the significant change in the normal mode displacement but due to the large excited state frequency changes of ν_{15}.

Supplementary material: The depolarization ratios for the major Raman lines of thiourea in acetonitrile at 252.7 nm excitation, the geometry structures of thiourea in S_0 and S_2 states are in the online version of this article.

IV. ACKNOWLEDGMENTS

This work was supported by the National Natural Science Foundation of China (No.21033002 and No.20803066) and the National Basic Research Program of China (No.2007CB815203).

TABLE V Resonance Raman intensity (in cm^{-1}) of thiourea in acetonitrile solution.

Peaks	At 245.9 nm			At 252.7 nm		
	Shift	Expt.	Calc.	Shift	Expt.	Calc.
ν_{15}	630	0	0	630	0	0
ν_6	744	8.3	10	742	7.42	10.3
ν_5	1063	0.5	0.86	1063	0.44	0.6
$2\nu_{15}$	1264	1.2	1.37	1262	1.404	1.30
ν_4	1403	0.545	0.77	1405	0.40	0.69
$2\nu_6$	1482	2.1	3.2	1483	2.3	2.1
$\nu_6+\nu_5$	1801	0.4	0.38	1801	0.24	0.20
$2\nu_{15}+\nu_6$	2001	0.5	0.61	2003	0.35	0.52
$\nu_6+\nu_4$	2141	0.52	0.28	2138	0.248	0.18
$4\nu_{15}$	2541	0.15	0.11	2545	0.162	0.142

[1] R. S. Mulliken, Phys. Rev. **41**, 751 (1932).
[2] D. H. Waldeck, Chem. Rev. **91**, 415 (1991) .
[3] R. A. McGill, J. K. Rice, A. P. Baranovski, J. C. Owrutsky, A. H. Lowrey, K. K. Stavrev, T. Tamm, and M. C. Zerner, Int. J. Quant. Chem. Symp. **30**, 383 (1996).
[4] B. L. Feringa, R. A. van Delden, N. Koumura, and E. M. Geertsema, Chem. Rev. **100**, 1789 (2000).
[5] L. Salem, J. Am. Chem. Soc. **12**, 87 (1979).
[6] V. Bonacic-Koutecky, P. Bruckmann, P. Hiberty, J. Koutecky, C. Leforestier, and L. Salem, Angew. Chem. Int. Ed. **14**, 575 (1975)
[7] C. E. Wulfman and S. Kumei, Science **172**, 1061 (1971)
[8] V. Bonacic-Koutecky, J. Am. Chem. Soc. **100**, 396 (1978).
[9] B. R. Brooks and H. F Schaefer, J. Am. Chem. Soc. **101**, 307 (1979).
[10] R. J. Buenker, V. Bonacic-Koutecky, and L. Pogliani, J. Chem. Phys. **73**, 1836 (1980).
[11] V. Bonacic-Koutecky, L. Pogliani, M. Persico, and J. Koutecky, Tetrahedron **38**, 741 (1982)
[12] P. Bruckmann and L. Salem, J. Am. Chem. Soc. **98**, 5037 (1976).
[13] C. M. Meerman-van Benthem, H. J. C. Jacobs, and J. J. C. Mulder, Nouv. J. Chim. **2**, 123 (1977).
[14] G. Orlandi, P. Palmieri, and G. Poggi, J. Am. Chem. Soc. **101**, 3492 (1979).
[15] I. D. L. Albert and S. Ramasesha, J. Phys. Chem. **94**, 6540 (1990).
[16] G. Orlandi and W. Siebrand, Chem. Phys. Lett. **14**, 19 (1972).
[17] L. D. Ziegler and B. S. Hudson, J. Chem. Phys. **79**, 1197 (1983).
[18] R. J. Sension, L. Mayne, and B. S. Hudson, J. Am. Chem. Soc. **109**, 5036 (1987).

DOI:10.1088/1674-0068/25/01/1-10

[19] R. J. Sension and B. S. Hudson, J. Chem. Phys. **90**, 1377 (1989).
[20] P. C. Gao, H. G. Wang, K. M. Pei, and X. Zheng, Chem. Phys. Lett. **445**, 173 (2007).
[21] X. M. Zhu, S. Q. Zhang, X. Zheng, and D. L. Phillips, J. Phys. Chem. A **109**, 3086 (2005).
[22] X. Zheng, Y. L. Li, and D. L. Phillips, J. Phys. Chem. A **108**, 8032 (2004).
[23] K. F. Weng, Y. Shi, X. Zheng, and D. L. Phillips, J. Phys. Chem. A **110**, 851 (2006).
[24] A. B. Myers, *Laser Techniques in Chemistry*, A. B. Myers and T. R. Rizzo, Ed., New York: Wiley, 325 (1995).
[25] S. Y. Lee and E. J. Heller, J. Chem. Phys. **71**, 4777 (1979).
[26] E. J. Heller, R. Sundberg, and D. Tannor, J. Phys. Chem. **86**, 1822 (1982).
[27] A. B. Myers and R. A. Mathies, *Biological Applications of Raman Spectroscopy*, T. G. Spiro, Eds., New York: Wiley, 2 (1987).
[28] M. J. Frisch, G. W. Trucks, H. B. Schlegel, G. E. Scuseria, M. A. Robb, J. R. Cheeseman, J. A. Montgomery Jr., T. Vreven, K. N. Kudin, J. C. Burant, J. M. Millam, S. S. Iyengar, J. Tomasi, V. Barone, B. Mennucci, M. Cossi, G. Scalmani, N. Rega, G. A. Petersson, H. Nakatsuji, M. Hada, M. Ehara, K. Toyota, R. Fukuda, J. Hasegawa, M. Ishida, T. Nakajima, Y. Honda, O. Kitao, H. Nakai, M. Klene, X. Li, J. E. Knox, H. P. Hratchian, J. B. Cross, C. Adamo, J. Jaramillo, R. Gomperts, R. E. Stratmann, O. Yazyev, A. J. Austin, R. Cammi, C. Pomelli, J. W. Ochterski, P. Y. Ayala, K. Morokuma, G. A. Voth, P. Salvador, J. J. Dannenberg, V. G. Zakrzewski, S. Dapprich, A. D. Daniels, M. C. Strain, O. Farkas, D. K. Malick, A. D. Rabuck, K. Raghavachari, J. B. Foresman, J. V. Ortiz, Q. Cui, A. G. Baboul, S. Clifford, J. Cioslowski, B. B. Stefanov, G. Liu, A. Liashenko, P. Piskorz, I. Komaromi, R. L. Martin, D. J. Fox, T. Keith, M. A. Al-Laham, C. Y. Peng, A. Nanayakkara, M. Challacombe, P. M. W. Gill, B. Johnson, W. Chen, M. W. Wong, C. Gonzalez, and J. A. Pople, *Gaussian 03*, Pittsburgh PA: Gaussian Inc., (2003).
[29] T. Ishiguro, E. I. Suzuki, A. Y. Hirakawa, and M. Tsuboi, J. Mol. Spectrosc. **83**, 360 (1980).
[30] J. E. Stewart, J. Chem. Phys. **26**, 248 (1957).
[31] A. Yamaguchi, R. B. Penland, S. Mitzushima, T. Lane, C. Curran, and J.V. Quagliano, J. Am. Chem. Soc. **80**, 527 (1958).
[32] K. Jensen and P. H. Nielsen, Acta Chem. Scand. **20**, 597 (1966).
[33] G. B. Aitken, J. L. Duncan, and G. B. Mequillan, J. Chem. Soc. A 2695 (1971).
[34] K. Srinivasan, S. Gunasekaran, and S. Krishnan, Spectrochimica Acta A **75**, 1171 (2010).
[35] H. Rostkowska, L. Lapinski, A. Khvorostov, and M. J. Nowak, J. Phys. Chem. A **107**, 6373 (2003).
[36] A. T. Kowal, J. Comput. Chem. **4**, 718 (2011).

DOI:10.1088/1674-0068/25/01/1-10